Sub-Doppler laser cooling using electromagnetically induced transparency

Peiru He, Phoebe M. Tengdin, Dana Z. Anderson, Ana Maria Rey, and Murray Holland

Phys. Rev. A **95**, 053403 — Published 9 May 2017

DOI: 10.1103/PhysRevA.95.053403

Sub-Doppler Laser Cooling using Electromagnetically Induced Transparency

Peiru He,[1,2] Phoebe M. Tengdin,[1] Dana Z. Anderson,[1] Ana Maria Rey,[1,2] and Murray Holland[1,2]

[1] *JILA and Department of Physics, University of Colorado, Boulder, Colorado 80309-0440, USA*
[2] *Center for Theory of Quantum Matter, University of Colorado, Boulder, Colorado 80309, USA*

We propose a sub-Doppler laser cooling mechanism that takes advantage of the unique spectral features and extreme dispersion generated by the phenomenon of electromagnetically induced transparency (EIT). EIT is a destructive quantum interference phenomenon experienced by atoms with multiple internal quantum states when illuminated by laser fields with appropriate frequencies. By detuning the lasers slightly from the "dark resonance", we observe that, within the transparency window, atoms can be subject to a strong viscous force, while being only slightly heated by the diffusion caused by spontaneous photon scattering. In contrast to other laser cooling schemes, such as polarization gradient cooling or EIT-sideband cooling, no external magnetic field or strong external confining potential is required. Using a semiclassical approximation, we derive analytically quantitative expressions for the steady-state temperature, which is confirmed by full quantum mechanical numerical simulations. We find that the lowest achievable temperatures approach the single-photon recoil energy. In addition to dissipative forces, the atoms are subject to a stationary conservative potential, leading to the possibility of spatial confinement. We find that under typical experimental parameters this effect is weak and stable trapping is not possible.

I. INTRODUCTION

Techniques for laser cooling and trapping of atoms have facilitated major advances in quantum science, and are now opening a window to the use of atomic systems for quantum information processing tasks [1–3]. Examples of these developments include the recent demonstrations of Bose-Einstein condensation and quantum degenerate Fermi gases, the coherent manipulation of individual atoms for the implementation of quantum logic [4], and the quantum simulation of model Hamiltonians such as the Bose-Hubbard model [5].

Despite the evident success of laser cooling methods, a variety of complex phenomena predicted in studies of strongly-correlated materials call for lower atomic temperatures than standard laser cooling techniques provide. For this reason, there is substantial interest in new laser cooling techniques that can achieve lower temperatures, higher densities, more rapid cooling, and be applicable to more general systems.

Doppler cooling is perhaps the most basic and fundamental of the laser cooling methods used in quantum gas experiments. This technique can cool a two-level systems to a temperature of the order of $\hbar\Gamma/k_B$ [6], where Γ is the natural linewidth of the atomic transition, and $\hbar$ and k_B are the reduced Planck's constant and Boltzmann's constant, respectively. The validity of this expression is limited to the case when $\hbar\Gamma$ exceeds the recoil energy with the recoil energy given by $E_r = \hbar^2k^2/2m$, where m is the atom's mass and k is the transition's wavevector. In order to reach sub-Doppler temperatures, other laser cooling methods such as Sisyphus cooling [7, 8] can be used that take advantage of a multilevel internal atomic structure. These typically allow the energy of an atom to be cooled to be of the order of the recoil energy [1]. Similar sub-Doppler cooling temperatures have been achieved using a three-level system illuminated by two pairs of standing waves [9–13].

Laser cooling techniques that achieve sub-recoil temperatures have generally required the use of dark-state resonances. These include velocity selective coherent population trapping (VSCPT) [14], as well as recently proposed techniques that combine electromagnetically induced transparency (EIT) [15] with sideband cooling [16]. The latter have enabled experimentalists to efficiently cool fermions in quantum gas microscopes [17, 18].

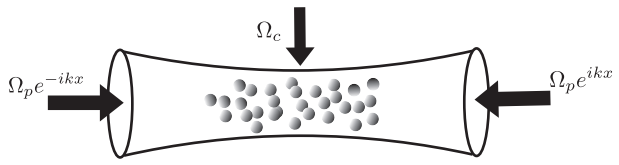

FIG. 1. The system we consider consists of atoms transversely confined so that they are able to move only in the x direction. The probe lasers consist of a pair of counter-propagating beams aligned with the x-axis with equal intensity as characterized by the Rabi frequency Ω_p. The coupling laser propagates perpendicularly to the probe beams as shown and has intensity characterized by the Rabi frequency Ω_c.

In this paper, we propose and analyze a laser cooling technique that combines the benefits of Doppler-cooling in multi-level atoms (in our case a three-level lambda system) with EIT. The distinctive dispersion relations of the EIT system have been well explored in non-linear optics, such as in the demonstration of extreme slow light in ultracold atomic gases [19]. The technique we use builds upon the well-known features of EIT to provide laser cooling to the recoil energy limit. Moreover, working with induced transparency suggests that this technique may provide effective cooling of high-density atomic clouds, a regime that challenges standard laser cooling methods [20–22]. As depicted in Fig. 1, atoms are illuminated by two counter-propagating probe beams and an additional coupling beam directed perpendicu-

larly to the other two. We show that in this system, laser cooling is possible when the probe lasers are slightly blue-detuned from the "dark resonance". As in all laser cooling methods, the equilibrium temperature is determined by a balance between the heating rate induced by spontaneous emission and the cooling rate generated by dissipative forces. The existence of a dark-state, together with the unique dispersion relations of the EIT system, modifies both rates: significantly reducing the heating rate by suppressing absorption, and simultaneously weakening dissipative forces. On balance, we find that the cooling achieved by the scheme can allow the atoms to reach final temperatures approaching the recoil energy limit.

In addition to these dissipative and fluctuating forces, we find the atom-probe interaction also imposes a periodic conservative optical potential. We find that the modulation depth of this conservative potential is comparable to the achievable temperatures, leading to the possibility of weak transient confinement and trapping that can significantly modify the dynamics.

The outline of the paper is the following: In Sec. II we introduce the proposed scheme including the atomic level structure and the laser configuration. We then present a brief review of the essential aspects of the EIT phenomenon and how this can be exploited to provide sub-Doppler cooling. In Sec. III, we discuss the physics behind the cooling mechanism and determine the achievable final temperatures. We use two different approaches: a semiclassical treatment that allows us to analytically derive expressions for the cooling rate, the capture range, the diffusion, and the equilibrium temperature; and a quantum Monte-Carlo wave function (MCWF) treatment that we use to numerically determine the capability of the proposed scheme to reach recoil-limited final temperatures. In Sec. IV, we consider the atomic motion and analyze the resulting spatial diffusion. Sec. V provides concluding remarks..

II. THE SETUP

Consider a stationary atom with three internal states, as shown in Fig. 2(a). The excited state, $|3\rangle$, can decay to two stable ground states, $|1\rangle$ and $|2\rangle$, with decay rates γ_1 and γ_2, respectively. The total decay rate of the excited state is thus $\gamma_3 \equiv \gamma_1 + \gamma_2$. The dipole allowed transition $|2\rangle \rightarrow |3\rangle$ with transition frequency ω_{23} is driven by a coupling laser with frequency ω_c, detuned from the atomic transition by $\Delta_c = \omega_c - \omega_{23}$, and with intensity characterized by the Rabi frequency Ω_c. Similarly, the transition $|1\rangle \rightarrow |3\rangle$, with transition frequency ω_{13}, is driven by a probe laser with frequency ω_p, detuned from the transition frequency by $\Delta_p = \omega_p - \omega_{13}$ and with Rabi frequency Ω_p.

This three-level scheme is a standard Λ-type EIT system. In our discussion, we denote the quantum projection operator $\hat{\sigma}_{ij} = |i\rangle\langle j|$, and the density matrix elements $\rho_{ji} = \langle \hat{\sigma}_{ij} \rangle$. The susceptibility for the probe laser field, defined as $\chi = \rho_{13}/\Omega_p$, is a function of the detuning Δ_p. Note that compared with the textbook definition of susceptibility, $\chi = P/\epsilon_0 E$, here, for simplicity, we have scaled the susceptibility by a constant $\frac{N\mu^2}{\hbar V \epsilon_0}$ (P is the polarization, E is the electric field amplitude, ϵ_0 is the electric constant, μ is the dipole moment, N is the atom number inside the medium, and V is the volume of the medium). Its real part, $\mathrm{Re}[\chi]$, characterizes refraction of the probe light, while its imaginary part, $\mathrm{Im}[\chi]$, characterizes absorption. When the two-photon resonance condition, $\Delta_p - \Delta_c = 0$, is fulfilled, there exists a perfect dark-state, $|\mathrm{Dark}\rangle = (\Omega_p|2\rangle - \Omega_c|1\rangle)/\sqrt{\Omega_p^2 + \Omega_c^2}$, for which the $\mathrm{Im}[\chi]$ vanishes and there is no absorption at all. In Fig. 2(b), we plot $\chi(\Delta_p)$ (solid and dashed lines) in the parameter region $\Omega_p, \Omega_c \ll \gamma_3$ with the assumption that $\Delta_c = 0$. Centered around the zero absorption point, $\Delta_p = 0$, is a detuning window of characteristic width $2(\Omega_p^2 + \Omega_c^2)/\gamma_3$ where absorption is significantly suppressed.

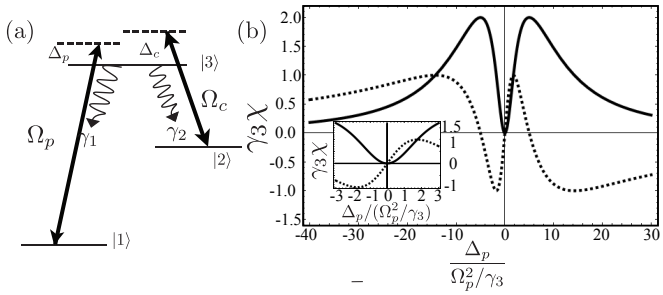

FIG. 2. (a) Lambda-type three-level atoms driven by two laser beams. (b) The real (solid line) and imaginary (dashed line) parts of the susceptibility χ are shown as a function of detuning Δ_p for the case $\Delta_c = 0$. The $\mathrm{Re}[\chi]$ characterizes refraction of the probe light, while the $\mathrm{Im}[\chi]$ characterizes absorption. The inset magnifies the small detuning region to highlight the behavior of the susceptibility in the transparency window. The parameters used for the plot are, $\Omega_p = 10E_r/\hbar$, $\Omega_c = 400E_r/\hbar$ and $\gamma_3 = 2000E_r/\hbar$.

Although the susceptibility properties are well-understood for three-level EIT systems, they have not to our knowledge been fully applied to the case of the laser-cooling of free-space atoms. A feature of particular interest in the context of laser cooling is the potentially reduced heating rate due to suppressed spontaneous emission in the absorption dip, as compared to the one seen in the absence of EIT. In this work, we study the cooling process in the simplest case of a one-dimensional system consisting of an ensemble whose atoms can only move along the x-axis. Let us now consider the effects of atom motion and the effects of the spatial variation of the applied fields.

We assume that the probe consists of two z-linear-polarized counter-propagating laser beams with equal frequency ω_p traveling in the positive and negative x-

directions. The coupling beam is a z-polarized traveling wave propagating along the y direction with frequency ω_c. The total electric field in the z direction is therefore given by $E_z = 2E_p e^{i\omega_p t}\cos kx + E_c e^{i\omega_c t} + \text{c.c.}$, where $k = \omega_p/c \approx \omega_{13}/c$ is the wavevector of the probe. In the interaction picture, the effective probe Rabi frequency $2\Omega_p \cos(kx)$ is therefore position dependent, while the coupling beam Rabi frequency Ω_c is constant in space. Both Ω_p and Ω_c are proportional to the corresponding electric field amplitudes E_p and E_c, which, without loss of generality, can be taken to be real.

For the sake of simplicity we consider the case of a sufficiently dilute gas so that interactions (collisions, photon reabsorption, radiation pressure, etc.) can be neglected. Consequently the dynamics can be modeled using a single-atom Hamiltonian. The Hamiltonian $\hat{H}$ consists of two terms, the external part $\hat{H}_{\text{ext}}$ that describes the external degrees of freedom and accounts for atomic motion, and the internal part $\hat{H}_{\text{int}}$ that describes the internal atomic levels. We will focus on the special case $\Delta_c = 0$, although it should be emphasized that cases with $\Delta_c \neq 0$ yield qualitatively similar results with respect to the final temperature. In the presence of dissipation, the evolution of the system is described by the Born-Markov quantum master equation written in terms of the density matrix $\hat{\rho}$:

$$\begin{aligned}
\hat{H} &= \hat{H}_{\text{ext}} + \hat{H}_{\text{int}} \\
\hat{H}_{\text{ext}} &= \frac{\hat{p}^2}{2m} \\
\hat{H}_{\text{int}} &= \hbar\Delta_p\hat{\sigma}_{11} + \hbar\left[2\Omega_p\cos(k\hat{x})\hat{\sigma}_{13} + \Omega_c\hat{\sigma}_{23} + \text{h.c.}\right] \\
\frac{d\hat{\rho}}{dt} &= \frac{i}{\hbar}[\hat{\rho},\hat{H}] + \gamma_1\int_{-1}^{1} du\,\mathcal{N}_1(u)\mathcal{L}[\hat{\sigma}_{13}e^{iku\hat{x}}]\hat{\rho} \\
&\quad + \gamma_2\int_{-1}^{1} du\,\mathcal{N}_2(u)\mathcal{L}[\hat{\sigma}_{23}e^{ik'u\hat{x}}]\hat{\rho}. \qquad (1)
\end{aligned}$$

where the Lindblad superoperator $\mathcal{L}[\hat{O}]\hat{\rho} = \frac{1}{2}(2\hat{O}\hat{\rho}\hat{O}^\dagger - \hat{O}^\dagger\hat{O}\hat{\rho} - \hat{\rho}\hat{O}^\dagger\hat{O})$ accounts for dissipative processes, and k' is the wavevector associated with transition $|3\rangle \rightarrow |2\rangle$. Here, $\mathcal{N}_{1,2}(u)$ parametrizes the normalized dipole radiation pattern projected along the x axis [23].

III. COOLING MECHANISM

A. Semiclassical treatment for a weak probe field

We break the analysis into separate considerations of two parameter regimes; the weak probe, $\Omega_p \ll \Omega_c \ll \gamma_3$, and the strong probe, $\Omega_c \ll \Omega_p \ll \gamma_3$. Here we begin with the weak probe regime where the cooling mechanism can be more easily understood and where it is possible to derive analytic expressions for the equilibrium temperature and the capture range (*i.e.* the range of atomic velocities that can be efficiently cooled). The discussion of the strong probe beam case follows in the next section along with an analysis of the resulting impact of the optical fields on the dynamics of the atomic motion.

In the weak probe regime, the cooling mechanism is similar to Doppler cooling: a moving atom asymmetrically absorbs photons from the two probe beams due to the influence of the Doppler effect. If the atom is moving to the right with velocity v, it sees a Doppler shifted frequency from the left propagating beam $\omega_p + kv$, giving an effective detuning $\Delta_p + kv$, and from the right propagating beam, a frequency $\omega_p - kv$ and associated detuning $\Delta_p - kv$. In an absorption event, the atom's momentum is shifted by the momentum of the photon, $+\hbar k$ for the right propagating beam and $-\hbar k$ for the left propagating beam. On the other hand, when the excited atom undergoes spontaneous emission, the direction of the emitted photon is drawn randomly from a dipole radiation pattern, and the atom recoils in the opposite direction to the emitted photon. It is the net momentum transfer of absorption and emission cycles that cools or heats the atom.

In order to cool, it is necessary for the atom to preferentially absorb photons from the beam that is opposing its motion, rather than the co-propagating beam. In the ordinary Doppler cooling of a two-level atom, the absorption rate increases as the detuning approaches zero and is maximum on resonance. Thus, in order for Doppler cooling to function, it is required to detune to the *red* (lower frequency) of the resonance, so that the effect of the Doppler shift is in the correct direction. However, in our case (illustrated in Fig. 1), the transparency window has an inverted dependence on detuning and the absorption completely vanishes on resonance. Thus, by analogy, in this system one would expect that it is necessary for the probe beams to be detuned to the *blue* of the resonance for laser cooling to occur.

In order to describe the motional dynamics while accounting for EIT interference effects, we develop a semiclassical approach that treats the internal levels fully quantum mechanically, while expressing the atom's position and momentum by a classical phase-space coordinate, (x, p), derived from the averages $p = \langle\hat{p}\rangle$ and $x = \langle\hat{x}\rangle$. The semiclassical approximation requires the temperature to be sufficiently large that the typical atomic kinetic energy greatly exceeds the recoil energy.

The force seen by the atom depends on the susceptibility. The simplest expression occurs for the case of an atom at rest, which reaches a steady-state susceptibility given by

$$\chi(\Delta_p) \approx \frac{\Delta_p}{(\Omega_c^2 - \Delta_p^2) - i\Delta_p\gamma_3/2} \qquad (2)$$

where the approximation $\Omega_p \ll \Omega_c$ has been used corresponding to the weak probe limit. If the atom is not at rest, but is moving with velocity $v = p/m$, the atom is effectively illuminated by two plane waves with different detunings $\Delta_p \pm kv$, split by the Doppler shift. In the weak probe regime, ρ_{13} can be derived to lowest order in Ω_p/Ω_c by superimposing these two counter-propagating

beams separately (see Appendix. A).

$$\rho_{13} \approx \Omega_p[e^{-ikx}\chi(\Delta_p - kv) + e^{ikx}\chi(\Delta_p + kv)] \quad (3)$$

The force on the atom is defined as the negative spatial derivative of the Hamiltonian.

$$\frac{dp}{dt} = \frac{d\langle\hat{p}\rangle}{dt} = -\langle\frac{\partial\hat{H}}{\partial\hat{x}}\rangle = 4\hbar k\sin(kx)\Omega_p\,\mathrm{Re}[\rho_{13}] \quad (4)$$

Substituting the expression for ρ_{13} as given in Eqn. (3) yields

$$\frac{dp}{dt} \approx 4\hbar k|\Omega_p|^2\sin(2kx)\,\mathrm{Re}[\chi(\Delta_p)] - 4\hbar|\Omega_p|^2 kv(1+\cos(2kx))\partial_{\Delta_p}\,\mathrm{Im}[\chi(\Delta_p)] \quad (5)$$

where we have assumed the ultracold limit $kv \ll \Delta_p$.

The first term in Eqn. (5) is the conservative dipole force, which averages to zero over a wavelength and which we neglect because its magnitude is small in the weak probe limit under consideration. This force, however, is relevant for strong probe fields and will be discussed in Sec. IV.

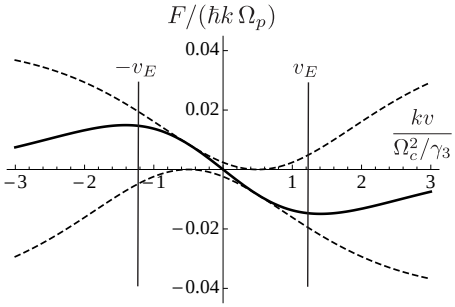

FIG. 3. Friction forces as a function of atom velocity. The two radiation forces (dashed lines) exerted by the two counter-propagating beams give rise to the net friction force (solid line). For blue-detuned probe beams, atoms with positive velocities experience a negative force and vice versa, corresponding to cooling. The magnitude of the friction force is maximized for atoms traveling at the critical velocity $\pm v_E$ shown, which determines the capture range. The parameters used were $kx = 0$, $\Delta_p = 40E_r/\hbar$, $\Omega_p = 20E_r/\hbar$, $\Omega_c = 400E_r/\hbar$ and $\gamma_3 = 2000E_r/\hbar$.

The second term in Eqn. (5) is the radiation force which gives rise to a velocity-dependent dissipative force, as shown in Fig. 3. For small absolute velocities, the radiation force is approximately linear, and the negative of the slope gives rise to the friction coefficient, denoted by $\eta(x)$. As the velocity increases, the dependence of the force on velocity becomes non-linear and a complicated expression is needed to describe the friction force. The "capture range" refers to the range of velocities which can be effectively cooled, and is defined by $-v_E < v < v_E$, where the critical velocity $\pm v_E$ corresponds to the maximum magnitude of the friction force. In the weak probe regime and in the limit of small probe detuning $\Delta_p \ll \Omega_c^2/\gamma_3$, the critical velocity is approximately $v_E \approx \Omega_c^2/(\gamma_3 k)$.

We find the friction coefficient $\eta(x)$ averaged over one wavelength is given by

$$\eta \equiv \overline{\eta(x)} \approx \frac{\hbar k^2}{m}\frac{16\gamma_3\Delta_p\Omega_p^2(\Omega_c^4 - \Delta_p^4)}{\left(4(\Omega_c^2 - \Delta_p^2) + \gamma_3^2\Delta_p^2\right)^2}, \quad (6)$$

and thus on average $dp/dt \approx -\eta p$. The friction coefficient η is plotted in Fig. 4. For blue detuning, $\Omega_c > \Delta_p > 0$, the friction coefficient is positive, $\eta > 0$, meaning that the rate of change of momentum is consistent with losing energy, and thus the system cools. However, for red detuning $-\Omega_c < \Delta_p < 0$, we find a negative friction coefficient, $\eta < 0$, which means that energy is transferred to the atoms from the photons, and correspondingly the system is heated.

Now we turn to a discussion of the role of fluctuations which, in concert with the friction forces just considered, determines the steady-state temperature. There are two main heating sources [24]: the first one arises from the random momentum kicks that the atom receives when it spontaneously emits a photon and recoils; the second arises from the zero-point fluctuations of the atomic dipole moment (due to the interaction with vacuum modes of the radiation field) in the presence of electric field gradients [25]. This effect is also intimately associated with spontaneous emission. In order to account for both of these two processes, we include a stochastic term $\hat{\xi}(t)$ in the equation of motion

$$\frac{dp}{dt} = -\eta p + \hat{\xi}(t)\,, \quad (7)$$

which satisfies the time averaged behavior of a white noise source, *i.e.* $\langle\hat{\xi}(t)\rangle = 0$, and $\langle\hat{\xi}(t)\hat{\xi}^\dagger(t')\rangle = 2D\delta(t-t')$ where D is the diffusion constant [26]

$$2D = \frac{d\langle\hat{p}^2\rangle}{dt} - 2\langle\hat{p}\rangle\langle\frac{d\hat{p}}{dt}\rangle\,. \quad (8)$$

$\mathcal{N}_{1,2}(u)$ depends on the specific quantum numbers of the transition, and has a minor effect on the numerical value of the diffusion constant. Thus for simplicity, we will assume the momentum kicks arising from spontaneous emission happen only along the $\pm x$ directions and with equal probability, that is $\mathcal{N}_{1,2}(u) = \frac{1}{2}\delta(u+1) + \frac{1}{2}\delta(u-1)$. Using this prescription, we obtain D by solving the master equation Eqn.(1) in the weak probe limit, giving

$$2D \approx \frac{\gamma_3}{\gamma_1}\frac{4\hbar^2\Omega_p^2\Delta_p^2(k^2\gamma_1 + k'^2\gamma_2)}{(\Omega_c^2 - \Delta_p^2)^2 + (\frac{\Delta_p\gamma_3}{2})^2} = \frac{4\gamma_3\hbar^2k^2\Omega_p^2\Delta_p^2(1 + c_k(1/c_\gamma - 1))}{(\Omega_c^2 - \Delta_p^2)^2 + (\frac{\Delta_p\gamma_3}{2})^2}, \quad (9)$$

where $c_\gamma = \gamma_1/\gamma_3$ and $c_k = (k'/k)^2$.

Determined by Eqn. (7), the momentum square is given by

$$p^2(t) = p^2(0)e^{-2\eta t} + \frac{D}{\eta}(1 - e^{-2\eta t}). \quad (10)$$

The characteristic cooling time can be read-off from the time constant of the exponentials in Eqn. (10), giving a value of $1/\eta$. The characteristic number of photons, N, scattered in this cooling time can then be obtained as

$$N = \frac{\gamma_3 \rho_{33}}{\eta} \approx \frac{\hbar}{2}\frac{\gamma_3}{\gamma_1}\frac{(\gamma_3/2)^2 + (\Omega_c^2/\Delta_p - \Delta_p)^2}{\Delta_p(\Omega_c^4/\Delta_p^4 - 1)}\frac{1}{E_r} \approx \frac{\hbar\Delta_p\gamma_3}{2\gamma_1 E_r}. \tag{11}$$

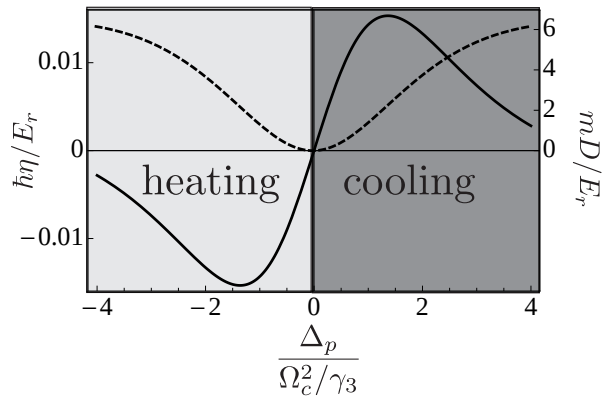

FIG. 4. Friction coefficient η (solid line) and diffusion coefficient D (dashed line) as a function of detuning. Both the friction and diffusion coefficients are zero at $\Delta_p = 0$. The friction, η, reaches a maximum at approximately $\Delta_p = 2\Omega_c^2/\gamma_3$, while the diffusion, D, is maximized at approximately $\Delta_p = \Omega_c$. The parameters used were, $\Omega_p = 20E_r/\hbar$, $\Omega_c = 400E_r/\hbar$ and $\gamma_3 \approx \gamma_1 = 2000E_r/\hbar$

.

According to Eqn. (10), the equilibrium temperature is found by comparing the relative magnitude of the cooling rate η and the diffusion D:

$$k_B T = \frac{D}{m\eta} = \frac{\hbar}{2}\frac{(\gamma_3/2)^2 + (\Omega_c^2/\Delta_p - \Delta_p)^2}{\Delta_p(\Omega_c^4/\Delta_p^4 - 1)}(1 + \frac{c_k}{c_\gamma} - c_k). \tag{12}$$

As an explicit example, we consider the commonly used alkali atom ^{87}Rb, where it is possible to implement the EIT scheme by choosing $|1\rangle = |5^2S_{1/2}, F = 1\rangle$, $|2\rangle = |5^2S_{1/2}, F = 2\rangle$, and $|3\rangle = |5^2P_{3/2}, F = 2\rangle$, satisfying $k \approx k'$. In this configuration, $\gamma_1 = \gamma_2 = 3.03\,\mathrm{MHz}$. Typical values of the Rabi frequencies and detunings are $\Omega_c = 1\mathrm{MHz}$, $\Omega_p = 0.1\mathrm{MHz}$, and $\Delta_p = 0.1\mathrm{MHz}$. Substituting these values into Eqn. (12) in the paper, the final cooling temperature is estimated to be $0.83\,\mu\mathrm{K}$. Note that cooling is still possible even though γ_2 is present, although the final temperature is increased. It should be emphasized that when $\gamma_2 \gg \gamma_1$, the final temperature may be higher than the Doppler temperature, so that the cooling is no longer efficient. Therefore, in order to avoid extra heating from γ_2, a system with small γ_2 is favorable to perform this EIT cooling method. In some special cases where $\gamma_1 \gg \gamma_2$, Eqn. (12) can be simplified as

$$k_B T = \frac{\hbar}{2}\frac{(\gamma_3/2)^2 + (\Omega_c^2/\Delta_p - \Delta_p)^2}{\Delta_p(\Omega_c^4/\Delta_p^4 - 1)} \approx \frac{\hbar}{2}[\frac{1}{4}(\frac{\gamma_3}{\Omega_c^2})^2\Delta_p^3 + \Delta_p] \approx \frac{\hbar\Delta_p}{2}. \tag{13}$$

We have validated Eqn. (12) by establishing its consistency with full semiclassical numerical simulations utilizing the c-number Langevin method, as described in detail in Appendix. B. For the numerical simulations it was not necessary to make the weak probe approximations, or to take the ultracold limit, as was required to allow tractable analytic expressions to be derived in the formulas we have just presented.

It should be emphasized that three conditions are required for Eqn. (12) to be valid.

1. $\Delta_p \ll 2\Omega_c^2/\gamma_3$. This ensures the detuning is confined to the blue side of the dark absorption dip.

2. $kv \ll \Delta_p$ for thermal velocities. This ensures the Doppler shift is not too large in comparison with the probe detuning. This requirement corresponds to the constraint that the friction and diffusion coefficients should be constant and not depend on velocity.

3. $k_B T \gg E_r$, that is, the thermal energy exceeds the recoil energy. This is due to the fact that a semiclassical treatment has been used. Should this condition not be met, a fully quantum mechanical treatment of the motional wavefunction would be necessary.

Although the first of these conditions is always required, it may be possible to relax the second and third conditions and still achieve laser cooling using this EIT approach. In the next section, we present a numerical treatment which demonstrates this more general theory case.

B. Quantum Mechanical Treatment

In parameter regimes where the predicted thermal energy from the semiclassical treatment approaches the recoil energy, the semiclassical method fails and the steady-state temperature must be found by solving the density matrix quantum mechanically, e.g. treating the external degrees of freedom (momentum and position) also as operators. However, without any simplification, it becomes difficult to solve the dynamics due to the large number of relevant basis states: if the momentum is in the range of $-N\hbar k$ to $N\hbar k$ with a discrete step $\hbar k$, the density matrix scales as N^2. However, the Monte-Carlo wavefunction (MCWF) method [28], which is based on the propagation of stochastic differential equations, reduces the computation complexity by requiring the storage of wavefunctions, which only scale as N, at the cost of computing an ensemble of simulated trajectories. The

MCWF method has shown to be equivalent to the density matrix description and has been applied to a wide variety of quantum optics problems, including laser cooling. Here, we use the MCWF method to accurately determine the minimum reachable temperature. Details of the numerical procedure are presented in Appendix. C.

In order to determine the minimum reachable temperature and validate the consistency of the various approximations made in deriving the analytic formulas, we performed a numerical study using a set of experimentally reasonable parameters. Fig. 5 summarizes the main results. It shows comparisons between the analytical model and two different numerical solutions, one based on the c-number Langevin treatment of the semiclassical equations, and the other based on the MCWF treatment of the full quantum solutions. All of them are consistent for parameters in which the equilibrium temperature is much greater than the recoil temperature. Discrepancies between the analytical formula and the result from MCWF are apparent when $\Delta_p \sim E_r$, as anticipated in the discussion presented in Sec. III(A). We note that when Δ_p approaches zero the observed temperature is close to the recoil limit rather than below it. This is in direct contradiction to Eqn. (12) that predicts no lower limit.

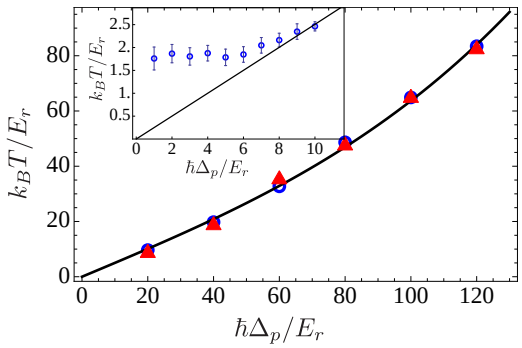

FIG. 5. Final temperature reached as a function of the detuning. The parameters were $E_r/\hbar = 5\text{kHz}$, $\Omega_c = 2\text{MHz} = 400\text{E}_\text{r}/\hbar$, $\Omega_p = 100\text{kHz} = 20\text{E}_\text{r}/\hbar$, $\gamma_3 \approx \gamma_1 = 10\text{MHz} = 2000\text{E}_\text{r}/\hbar$. The truncated momentum basis ranged from $-50\hbar k$ to $50\hbar k$. The analytical formula (solid line), semiclassical numerical results (triangle) and MCWF numerical results (circle) are compared. They agree well when the detuning is significantly larger than the recoil energy, but discrepancies appear when the detuning is near the recoil energy, as shown in the inset plot. The standard errors for the small detuning points are in the order of 0.1 as shown by the error bars in the inset, while the standard errors for large detunings points are in the order of 0.01, which are too small to be depicted in the large plot.

IV. ATOMIC MOTION

In the weak probe regime, the conservative force that arises from the standing wave light field does not play a significant role, but this ceases to be true when strong probe fields are considered. In general, the induced lattice potential must be included. The important question is then: can an atom be trapped in and confined to a single site of the lattice, and if so, how long will it remain trapped when subjected to the momentum kicks induced by random fluctuations? The random fluctuations compete with friction forces that cool the atom and may result in localization for considerable periods of time. One may expect that the effectiveness of a trap in confining an atom would be determined by the ratio of the lattice depth to the temperature at equilibrium. Assuming a small Doppler shift, $kv \ll \Delta_p$, the periodic potential $V(x)$ is given by

$$V(x) \approx \frac{\hbar\Delta_p}{1 + (\Omega_c/2\tilde{\Omega}_p)^2}, \tag{14}$$

where $\tilde{\Omega}_p = \Omega_p \cos(kx)$. This expression is valid in the regime of the usual operating conditions of small probe detuning, $\Delta_p \ll \Omega_c^2/\gamma_3$. The lattice depth V_d can be calculated by $V_d = |V(0) - V(\pi/2k)|$.

The friction coefficient and the temperature in this strong probe limit are difficult to derive analytically therefore we calculate them as observables from the numerical simulations. Fig. 6(a) and Fig. 6(b) show η and k_BT/V_d as a function of the probe intensity $2\Omega_p$ ranging from the weak probe limit $\Omega_c/20$ to the strong probe limit $2.5\Omega_c$. While η grows quadratically with Ω_p in the weak probe regime, it grows at a slower rate when Ω_p becomes comparable or larger than Ω_c. In the weak probe limit, the final kinetic energy is not affected by Ω_p and the optical lattice potential effectively vanishes; in the strong probe limit, the lattice depth becomes large but the final kinetic energy also increases dramatically. The comparison between the equilibrium temperature and the lattice depth is found to be $k_BT > V_d$ for the conditions under consideration. The trajectories, obtained from the simulations, represent the atoms position x as a function of time t.

Each single atom starts with a velocity within the capture rage selected randomly from a high-temperature Maxwellian distribution. While its position is observed to change significantly at the beginning, gradually, the atom begins to be cooled and the position is observed to change at a slower rate. Finally, at about $t \sim 1/\eta$, the atom is cooled to steady-state and becomes weakly trapped in the induced lattice. These general features are illustrated in Fig. 6(c) where trajectories are clearly visible that oscillate back and forth, demonstrating the trapping of atoms in a single site. However, since the temperature is never significantly below the lattice depth, this trapping is transient, and the diffusion drives the atom out of a site, after which it may gain sufficient energy to fly over several sites before being recaptured. Fig. 6(d) shows the position-dependent density distribution. The histogram is made by recording the position of each atom after reaching equilibrium in the simulation. The solid line represents the analytically derived density distribution. By assuming that the thermodynamics of the equilibrated atomic gas obeys the Boltz-

mann distribution, the spatially variant density distribution is found to be proportional to $\exp(-V(x)/k_BT)$, where $k_BT \approx 70E_r = 1.75V_d$ is read from Fig. 6(b). These density distributions found by the two methods agree well. Fig. 6(d) apparently shows that the atoms are not completely trapped at the bottom of the lattice, which is consistent with the conclusions drawn from Fig. 6(b) and Fig. 6(c) and suggests that the trapping effect by this mechanism is weak.

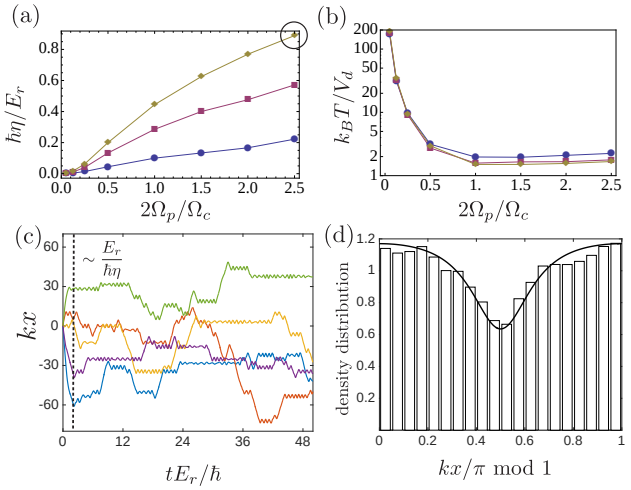

FIG. 6. (a)The friction coefficient as a function of $2\Omega_p/\Omega_c$, with the parameters $\gamma_3 \approx \gamma_1 = 2000E_r/\hbar$ and $\Omega_c = 400E_r/\hbar$ at three detunings within the absorption dip; they are $\Delta_p = 10E_r/\hbar$ (round), $\Delta_p = 30E_r/\hbar$ (square), and $\Delta_p = 50E_r/\hbar$ (diamond) respectively. (b)The ratio between the lattice depth and the final kinetic energy as a function of $2\Omega_p/\Omega_c$, with the same simulation parameters as (a). (c) This subfigure shows 5 trajectories, representing the atom position x as a function of time. The simulation parameters are extracted from the circle in (a). At about $t \sim 1/\eta$, as shown by the dashed line, the atom is cooled down. After short periods of weak trapping within the wells of the lattice, the atom may gain sufficient energy to propagate over multiple sites before being cooled and recaptured. (d) This subfigure shows the position dependence of the density distribution, with the same parameters as used in (c). The histogram is obtained from the simulations by recording the position of each atom after reaching equilibrium. The solid line represents the density distribution that is analytically derived by assuming that the thermodynamics of the equilibrated atomic gas obeys the Boltzmann distribution.

V. CONCLUSIONS

We have proposed and analyzed a novel cooling mechanism based on a Lambda-type EIT system, where heating of the atoms is largely suppressed by destructive quantum interference. We have shown in the weak probe beam regime that by blue detuning the laser beams it is possible to take advantage of the EIT reduced absorption window to cool down the atoms, and to reach sub-Doppler final temperatures set by the detuning instead of the atoms' decay rate. We developed and analyzed the results of a model obtained using a semiclassical approach, which we compared with the solutions of the full quantum dynamics using a MCWF method. Discrepancies appeared when the detuning approached zero, where the final temperature was comparable to the recoil energy. In the strong probe beam region, we derived the depth of the optical lattice potential experienced by the atom, and compared it with the final temperatures. By computing the ratio of the final temperature to the lattice depth, we found that the atoms can be weakly trapped, which is consistent with the observed behavior of the atomic motion in the simulations.

In our discussion, we assumed that the atomic gas was dilute. In fact, it is often the case in laser-cooling experiments that the atomic gas is not in this regime, but is optically thick. Therefore, laser beams may be drastically attenuated as they propagate, and may be subject to strong non-linear optical effects. Consequently, in real systems, fewer atoms may be subject to the intended dissipative forces, which may significantly modify the efficacy and achievable temperatures. This adverse effect arising from photon absorption and dispersion in the optically thick sample could be significantly mitigated by the use of the absorption dip in the EIT transparency window as we have proposed. Furthermore, the degree of transparency is directly controllable by tuning the probe laser. It is worthy to note that although the cooling rate per atom is reduced as a result of the decrease of the detuning, it is possible for the total cooling rate for the whole system to remain roughly unchanged since more atoms may be cooled in such a transparent system.

Moreover, multi-atom interactions can be important in a dense gas, including ground state collisions, dipole-dipole interactions, light-assisted collisions, as well as the macroscopic radiation pressure forces that can limit the total number of atoms that can be trapped and cooled. Many of these interactions are mediated by photon emission, and hence could be largely suppressed by using the EIT absorption dip [29, 30]. Although we have not included calculations of multi-atom effects in this paper, the topic will be an interesting extension for future work.

In this paper, we have limited the discussion to one-dimensional (1D) systems, even though typical laser cooling applications often require 2D or 3D cooling. In the 1D scheme, one transverse coupling beam is employed to prevent the transfer of momentum from the laser into the direction that we wish to cool. This cooling method can be easily generalized to 2D, since the coupling beam can be aligned perpendicular to the plane in which the atomic motion takes place. The extension to 3D cooling is not so obvious. For 3D cooling, the radiation force induced by the coupling beam should be taken into account, which might have to be balanced by applying an additional force. A simple way to generalize the 1D cooling scheme to 3D cooling is by alternately cooling the three orthogonal directions successively. However, the efficiency of this generalization needs more careful anal-

ysis.

We would like to emphasize that although we have focussed on employing laser fields that have constant frequency, a more general situation could be beneficial. For example, even though the capture range is limited by the Rabi frequency of the coupling laser and the linewidth of the excited state, strategies could be implemented in which these are swept in time to capture large numbers of hot atoms, and later to cool them to very low temperatures. It will be interesting to explore such general approaches.

We acknowledge helpful discussions with Minghui Xu. The material is based upon work supported by the National Science Foundation under Grant Numbers PHY1125844 & PHY1404263, the National Institute of Standards and Technology, the DARPA QuASAR program, and the Air Force Office of Scientific Research under Grant Number FA9550-14-1-0327.

[1] C. N. Cohen-Tannoudji, Rev. Mod. Phys. **70**, 707 (1998).
[2] S. Chu, Rev. Mod. Phys. **70**, 685 (1998).
[3] W. D. Phillips, Rev. Mod. Phys. **70**, 721 (1998).
[4] C. Monroe, D. M. Meekhof, B. E. King, W. M. Itano, and D. J. Wineland, Phys. Rev. Lett. **75**, 4714 (1995).
[5] M. Greiner, O. Mandel, T. Esslinger, T. Hansch, and I. Bloch, Nature **415**, 39 (2002).
[6] Y. Castin, H. Wallis, and J. Dalibard, J. Opt. Soc. Am. B **6**, 2046 (1989).
[7] J. Dalibard and C. Cohen-Tannoudji, J. Opt. Soc. Am. B **6**, 2023 (1989).
[8] D. J. Wineland, J. Dalibard, and C. Cohen-Tannoudji, J. Opt. Soc. Am. B **9**, 32 (1992).
[9] R. Gupta, C. Xie, S. Padua, H. Batelaan, and H. Metcalf, Phys. Rev. Lett. **71**, 3087 (1993).
[10] D. R. Fernandes, F. Sievers, N. Kretzschmar, S. Wu, C. Salomon, and F. Chevy, EPL (Europhysics Letters) **100**, 63001 (2012).
[11] A. T. Grier, I. Ferrier-Barbut, B. S. Rem, M. Delehaye, L. Khaykovich, F. Chevy, and C. Salomon, Physical Review A **87**, 063411 (2013).
[12] F. Sievers, N. Kretzschmar, D. R. Fernandes, D. Suchet, M. Rabinovic, S. Wu, C. V. Parker, L. Khaykovich, C. Salomon, and F. Chevy, Physical Review A **91**, 023426 (2015).
[13] G. Morigi and E. Arimondo, Physical Review A **75**, 051404 (2007).
[14] A. Aspect, E. Arimondo, R. Kaiser, N. Vansteenkiste, and C. Cohen-Tannoudji, Phys. Rev. Lett. **61**, 826 (1988).
[15] K.-J. Boller, A. Imamoğlu, and S. E. Harris, Phys. Rev. Lett. **66**, 2593 (1991).
[16] G. Morigi, J. Eschner, and C. H. Keitel, Phys. Rev. Lett. **85**, 4458 (2000).
[17] E. Haller, J. Hudson, A. Kelly, D. A. Cotta, B. Peaudecerf, G. D. Bruce, and S. Kuhr, Nature physics **11**, 738 (2015).
[18] G. J. A. Edge, R. Anderson, D. Jervis, D. C. McKay, R. Day, S. Trotzky, and J. H. Thywissen, Phys. Rev. A **92**, 063406 (2015).
[19] L. V. Hau, S. E. Harris, Z. Dutton, and C. H. Behroozi, Nature **397**, 594 (1999).
[20] A. Gallagher and D. E. Pritchard, Phys. Rev. Lett. **63**, 957 (1989).
[21] P. S. Julienne and F. H. Mies, JOSA B **6**, 2257 (1989).
[22] T. Walker, D. Sesko, and C. Wieman, Phys. Rev. Lett. **64**, 408 (1990).
[23] M. Xu, S. B. Jäger, S. Schütz, J. Cooper, G. Morigi, and M. J. Holland, Phys. Rev. Lett. **116**, 153002 (2016).
[24] J. P. Gordon and A. Ashkin, Phys. Rev. A **21**, 1606 (1980).
[25] D. C. McKay and B. DeMarco, Reports on Progress in Physics **74**, 054401 (2011).
[26] C. Gardiner and P. Zoller, Quantum noise, Vol. 56 (Springer Science & Business Media, 2004).
[27] SupplementalMaterial, .
[28] K. Mølmer, Y. Castin, and J. Dalibard, J. Opt. Soc. Am. B **10**, 524 (1993).
[29] D. E. Chang, V. Vuletić, and M. D. Lukin, Nature Photonics **8**, 685 (2014).
[30] K. E. Gibble, S. Kasapi, and S. Chu, Optics Letters **17**, 526 (1992).

Appendix A: Derivation of the coherence ρ_{13}

The coherence ρ_{13} can be obtained by solving the master equation in Eqn. (1). For the case of an atom at rest, it is straightforward to derive that

$$\rho_{13} = \frac{2\Omega_c^2\Delta_p\Omega_p\left(2\gamma_2\Omega_p^2+\gamma_1\left(2\Omega_c^2+i\gamma_3\Delta_p-2\Delta_p^2\right)\right)}{\gamma_1\Omega_c^2\left(4\left(-\Delta_p^2\left(2\Omega_c^2+\Omega_p^2\right)+\left(\Omega_c^2+\Omega_p^2\right)^2+\Delta_p^4\right)+\gamma_3^2\Delta_p^2\right)+\Omega_p^2\left(12\gamma_3\Omega_c^2\Delta_p^2+\gamma_2\left(4\left(\left(\Omega_c^2+\Omega_p^2\right)^2-\Omega_c^2\Delta_p^2\right)+\gamma_3^2\Delta_p^2\right)\right)}. \tag{A1}$$

This can be expanded to the sixth order of Ω_p in the limit that $\Delta_p \ll \Omega_c, \gamma_3$ as

$$\begin{aligned}\rho_{13} \approx & \frac{\Delta_p \Omega_p}{-i\gamma_3\Delta_p/2 + (\Omega_c^2 - \Delta_p^2)} - \frac{2\Delta_p\Omega_p^3\left(8\gamma_1\Omega_c^4 + \gamma_2\gamma_3\Delta_p\left(\gamma_3\Delta_p + 2i\Omega_c^2\right)\right)}{\gamma_1\left(2\Omega_c^2 + i\gamma_3\Delta_p\right)\left(-2\Omega_c^3 + i\gamma_3\Omega_c\Delta_p\right)^2} \\ & + \frac{2\Delta_p\Omega_p^5\left(8\gamma_1\gamma_2\gamma_3\Omega_c^4\Delta_p\left(\gamma_3\Delta_p + 2i\Omega_c^2\right) + 4\gamma_1^2\Omega_c^4\left(12\Omega_c^4 - \gamma_3^2\Delta_p^2\right) + \gamma_2^2\gamma_3\Delta_p\left(\gamma_3\Delta_p + 2i\Omega_c^2\right)^2\left(\gamma_3\Delta_p - 2i\Omega_c^2\right)\right)}{\gamma_1^2\Omega_c^4\left(2\Omega_c^2 - i\gamma_3\Delta_p\right)^3\left(2\Omega_c^2 + i\gamma_3\Delta_p\right)^2} \\ & + O(\Omega_p^7), \end{aligned} \tag{A2}$$

where the first three terms are on the first order, third order, and the fifth order of Ω_p, which can be labeled as O_1, O_3 and O_5 respectively. To compare the magnitude of these terms, we find

$$\begin{aligned}\frac{O_3}{O_1} &\approx -\frac{2\Omega_p^2}{\Omega_c^2} \\ \frac{O_5}{O_3} &\approx -\frac{3\Omega_p^2}{\Omega_c^2}, \end{aligned} \tag{A3}$$

where the approximation is valid when $\Delta_p \ll \Omega_c \ll \gamma_3$, which is the parameter regime of our interest. From the comparison, it is apparent that as long as $\Omega_p \ll \Omega_c$, it is sufficient to keep only the first order term, which yields Eqn. (2) in the main text

$$\chi(\Delta_p) = \frac{\rho_{13}}{\Omega_p} \approx \frac{\Delta_p}{(\Omega_c^2 - \Delta_p^2) - i\Delta_p\gamma_3/2}. \tag{A4}$$

To realize laser cooling, the probe laser is a standing wave. With the semiclassical assumption, an atom moving with velocity v experiences different frequencies of the counter-propagating lasers due to the Doppler shift. It is complicated to derive an exact solution of ρ_{13}. However, the derivation can be simplified based on the previous conclusion that the coherence ρ_{13} is approximately linear with the imposed weak probe lasers. Therefore higher order nonlinear terms can be neglected and it is reasonable to treat the two counter-propagating lasers seperately. Hence, ρ_{13} contains two parts, each obtained based on the linear coherence argument with the corresponding Doppler-shifted detuning, giving

$$\rho_{13} = \Omega_p e^{-ikx}\chi(\Delta_p - kv) + \Omega_p e^{ikx}\chi(\Delta_p + kv), \tag{A5}$$

as expressed in Eqn. (3) in the main text.

Appendix B: C-Number Langevin Method

In this method, the atomic momentum and position are treated semiclassically, and the dynamical equation of motion for the atomic momentum is augmented with a stochastic term. The weight of the stochastic fluctuation is set so that the resulting momentum diffusion agrees with that arising from quantum noise in a full quantum treatment of the same problem. In practice, this means that a single atom evolves according to Eqn. (B1), in which the differential equation for momentum p contains a Gaussian fluctuating stochastic process $\sqrt{2D}\,\xi^{\text{class}}$ that replaces the quantum noise operator $\hat{\xi}$ in the quantum Langevin equation (originally given in Eqn. (7) in the paper). The closed set of Ito stochastic differential equations to solve numerically are then given by

$$\begin{aligned}\frac{dp}{dt} &= 4\sin(kx)\Omega_p(\rho_{13} - \rho_{31}) + \sqrt{2D}\,\xi^{\text{class}} \\ \frac{dx}{dt} &= \frac{p}{m} \\ \frac{d\rho_{23}}{dt} &= -\frac{\gamma_3}{2}\rho_{23} + i(\rho_{33} - \rho_{22})\Omega_c - 2i\rho_{21}\Omega_p\cos(kx) \\ \frac{d\rho_{12}}{dt} &= i\Delta_p\rho_{12} - i\rho_{13}\Omega_c + 2i\rho_{32}\Omega_p\cos(kx) \\ \frac{d\rho_{13}}{dt} &= i\Delta_p\rho_{13} - \frac{\gamma_3}{2}\rho_{13} - i\rho_{12}\Omega_c + 2i(\rho_{33} - \rho_{11})\Omega_p\cos(kx) \\ \frac{d\rho_{22}}{dt} &= -i\Omega_c(\rho_{23} - \rho_{32}) + \gamma_2\rho_{33} \\ \frac{d\rho_{33}}{dt} &= -\gamma_3\rho_{33} + i\Omega_c(\rho_{23} - \rho_{32}) + 2i(\rho_{13} - \rho_{31})\Omega_p\cos(kx). \end{aligned} \tag{B1}$$

In order to solve these equations, a number of alternative algorithms are available, such as the Milstein method and the Runge-Kutta method. We have implemented various numerical algorithms and do not find our results to depend on the choice. In this paper, we have presented numerical calculations using the Euler-Maruyama method, which is a simple generalization of the Euler method for numerical integration to treat stochastic differential equations. Explicitly, the differential equation for the momentum is treated in the following way. Advancing the momentum over a numerical integration step of size Δt, we evaluate

$$\Delta p = 4\sin(kx)\Omega_p(\rho_{13}-\rho_{31})\Delta t + \sqrt{2D}\,\Delta\xi^{\rm class}\,. \tag{B2}$$

The random variable $\Delta\xi^{\rm noise}$ for each time step is treated as statistically independent and is found by sampling (using a numerically produced quasi-random number) from a normal distribution with zero mean and variance Δt. Together with the properties of the density matrix $\mathrm{Tr}\,\rho = 1$ and $\rho^\dagger = \rho$, the time dependence of all elements of the density matrix can be tracked.

Appendix C: Monte-Carlo Wave Function (MCWF) Method

The numerical procedure used to solve the quantum dynamics using the MCWF method is the following: the time-dependent wave function is expanded in terms of the basis $|i,\,p\rangle$. Here i denotes the internal states and p accounts for the quantized momentum along x axis. The momentum grid is specified as a family of momenta each separated by $\hbar k$, and with a central offset $\tilde{p}$, giving a grid of momentum basis states that range from $-N\hbar k+\tilde{p}$ to $N\hbar k+\tilde{p}$. We expand a general quantum state $|\psi(t)\rangle$ in this basis as

$$|\psi(t)\rangle = \sum_{p_n=-N\hbar k}^{N\hbar k}\sum_{i=1}^{3} c_{i,n}(t)|i,\,\tilde{p}+p_n\rangle \tag{C1}$$

To account for the dissipative processes induced by spontaneous emission, the non-Hermitian evolution is added to the Hamiltonian to give

$$\begin{aligned} H_{\rm eff} = \sum_{p_n=-N\hbar k}^{N\hbar k}\Big\{ &\sum_{i=1}^{3}\frac{(\tilde{p}+p_n)^2}{2m}|i,\,\tilde{p}+p_n\rangle\langle i,\,\tilde{p}+p_n| + \hbar\Delta_p|1,\tilde{p}+p_n\rangle\langle 1,\tilde{p}+p_n| \\ &+\hbar\Omega_p\big(|1,\tilde{p}+p_n\rangle\langle 3,\tilde{p}+p_{n+1}| + |1,\tilde{p}+p_n\rangle\langle 3,\tilde{p}+p_{n-1}| + \text{h.c.}\big) \\ &+\hbar\Omega_c\big(|2,\tilde{p}+p_n\rangle\langle 3,\tilde{p}+p_n| + \text{h.c.}\big) - \frac{i\hbar\gamma_3}{2}|3,\tilde{p}+p_n\rangle\langle 3,\tilde{p}+p_n|\Big\}, \end{aligned} \tag{C2}$$

where h.c. denotes the hermitian conjugate.

The wave function is evolved under Schrodinger's equation, giving coupled differential equations for the coefficients $c_{i,n}(t)$

$$\begin{aligned} \frac{d\,c_{1,n}(t)}{dt} &= -i\Big(\frac{(\tilde{p}+n\hbar k)^2}{2m\hbar}+\Delta_p\Big)c_{1,n}(t) - i\Omega_p\big(c_{3,n+1}(t)+c_{3,n-1}(t)\big) \\ \frac{d\,c_{2,n}(t)}{dt} &= -i\frac{(\tilde{p}+n\hbar k)^2}{2m\hbar}c_{2,n}(t) - i\Omega_c c_{3,n}(t) \\ \frac{d\,c_{3,n}(t)}{dt} &= -i\Big(\frac{(\tilde{p}+n\hbar k)^2}{2m\hbar}-\frac{i\gamma_3}{2}\Big)c_{3,n}(t) - i\Omega_p\big(c_{1,n+1}(t)+c_{1,n-1}(t)\big) - i\Omega_c c_{2,n}(t) \end{aligned} \tag{C3}$$

Numerically, we apply a second-order Runge-Kutta method to solve Eqn. (C3). A quantum jump (a single dissipative event) occurs at a time t when the norm of the wave function becomes smaller than a fixed initially produced random number that is drawn from a uniform distribution in the interval [0, 1]. For the special case that $\gamma_3 \approx \gamma_1 \gg \gamma_2$, the action of the quantum jump on the wavefunction is given by applying the rules

$$\begin{aligned} c_{1,n}(t) &\to c_{1,n}(t) = c_{3,n}(t) \\ c_{2,n}(t) &\to c_{2,n}(t) = 0 \\ c_{3,n}(t) &\to c_{3,n}(t) = 0 \\ \tilde{p}(t) &\to \tilde{p}(t) = \tilde{p}(t) \pm \hbar k \end{aligned} \tag{C4}$$

and the wave function is subsequently renormalized to unit norm. Whether the + or − is used is determined by flipping a coin, coinciding with the random direction of the emitted photon and leading to momentum diffusion in the quantum treatment. After each emission event, the atom is found in its ground state and the momentum distribution has been shifted by an amount $\hbar k$.